Reynolds Number Effect on Separation Structures at Normal Shock Wave/Turbulent Boundary-Layer Interaction

P. Doerffer*
Polish Academy of Sciences, Gdansk, Poland
and
U. Dallmann†
German Aerospace Research Establishment, Goettingen, Federal Republic of Germany

An experiment on normal shock wave/turbulent boundary-layer interaction is analyzed. The experiment is performed on a convex wall in a narrow wind tunnel at a wall Mach number $M_w = 1.47$ for the Reynolds numbers $Re_{\delta u} \times 10^{-4} = 5.5; 9.7; 13.1; 15.3$. The experiments indicate that due to this interaction the separated flowfield is highly three-dimensional. Static wall pressure measurements, pitot and static pressure surveys, and schlieren pictures support and complement a topological analysis of the flowfield structure based on oil-flow visualization. The non-unique dependence between a three-dimensional separated flowfield structure and its oil-flow pattern is emphasized. The complex topology of the separated flowfield is analyzed exhibiting a pronounced asymmetry with increasing Reynolds number.

Introduction

NORMAL shock wave/turbulent boundary-layer interaction (NSW/TBLI) is one of the gasdynamical problems where present interest is stimulated by its applicational importance. The effects of such an interaction are the increase of the aerodynamical drag and the possibility of buffet onset. At high enough Mach numbers of an undisturbed stream, separation is the natural consequence of the interaction. Therefore, an investigation of separation onset and its development is one of the main aims of the present work.

Most theoretical studies of NSW/TBLI treat purely two-dimensional flow cases and, therefore, it is a common practice to provide a two-dimensional interpretation of the experiments. Hence, it would be beneficial to minimize the deviation from a two-dimensional NSW/TBLI at least within the central region of the tunnel. However, there are principal difficulties in this respect due to the presence of side walls and, possibly, due to a three-dimensional, hydrodynamic instability of such high Reynolds number flows. In any case, one has to identify the three-dimensional effects that are found in the experiments.

Our interest in an experimental investigation and a topological analysis of NSW/TBLI has been motivated by the theoretical and experimental work of Bohning and Zierep.[1,2] One aim of their work was to find experimentally the range of Reynolds number and Mach number within which flow separation takes place in order to verify two-dimensional theoretical predictions. Doerffer and Zierep[3] provided further measurements to study the Reynolds number effect on NSW/TBLI on a curved wall for $M_w = 1.47$. Difficulties in the determination of separation complicated the interpretation of the data obtained. Therefore, the analysis of the separation process, the topological structure of the separated flowfield, and its changes due to Reynolds number variations are the subject of the present paper.

Nebbeling[4] investigated NSW/TBLI on a convex wall too. He used a tunnel that was three times wider than ours for investigating a Reynolds number and Mach number case close to our investigations. However, he did not analyze the three-dimensionality of the flow. Benay et al.[5] performed extensive three-color LDV-measurements in a transonic channel that had a pronounced swept hump. Therefore, this flow is a priori highly three-dimensional and it would be meaningless to apply two-dimensional physical models to explain their results. On the other hand, there is still a lack of physical understanding of three-dimensional phenomena that are always present in experiments in the shock-induced separated flow regions.

Measurement Arrangement and Methods

In the following, a brief description of earlier investigations[3,6-9] is given with a different view of the data that allows this paper to focus on the topological analysis of the Reynolds number dependent, three-dimensional, shock-induced *separated* flowfield.

The experimental investigation has been carried out at the Institut für Strömungslehre und Strömungsmaschinen at the Karlsruhe University, Federal Republic of Germany. The blowdown wind tunnel used is a short-duration, vacuum-type facility, having about 15 s run time.

The desired flowfield is obtained in a curved duct (Fig. 1). It is 50 mm wide and in the choking area it is about 150 mm high. At the convex wall the stream is accelerated to supersonic velocities. A local supersonic area is established that is terminated by a normal shock wave. This local supersonic area does not reach the upper wall, thus allowing the flow to choke at the exit section. The mass flow is therefore controlled by adjusting this area. Mass-flow variation alters the size of the supersonic area, hence the Mach number in front of the interaction as

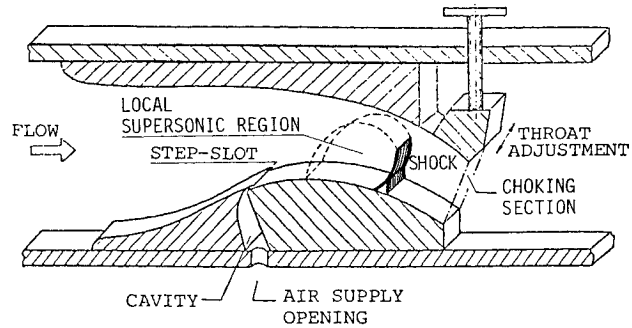

Fig. 1 Test section.

Presented as Paper 87-1370 at the AIAA 19th Fluid Dynamics, Plasma Dynamics and Lasers Conference, Honolulu, HI, June 8-10, 1987; received Feb. 9, 1988; revision received Sept. 21, 1988. Copyright © 1988 American Institute of Aeronautics and Astronautics, Inc. All rights reserved.

*Research Scientist, Institute of Fluid Flow Machinery.
†Branch Chief, DLR Institute for Theoretical Fluid Mechanics.

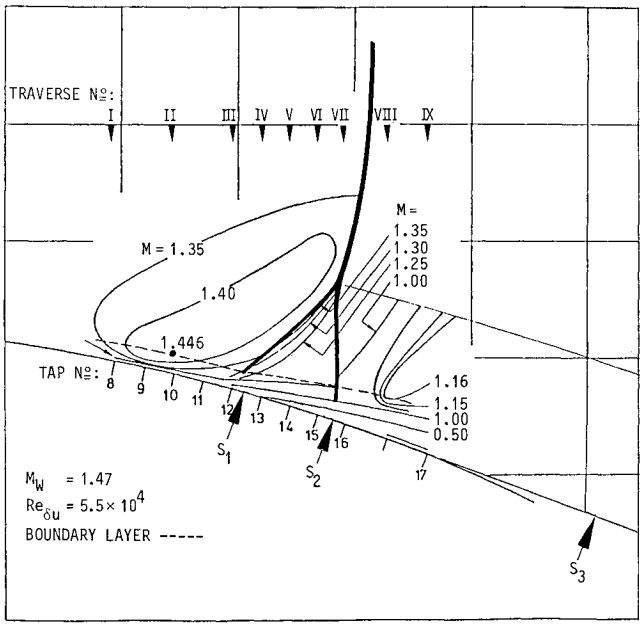

Fig. 2 Shock-wave configuration (from schlieren picture) and iso-Mach number lines for $M_w = 1.47$ and $Re_{\delta u} = 5.5 \times 10^4$.

well as the shock location are changed. This shock location is so sensitive to the interaction Mach number, that it is used to verify the flow repeatability.

In the experimental facility used, the stagnation parameters are equal to ambient conditions and therefore cannot be used as a means to vary the Reynolds number. The characteristic length for Re in the interaction problem is the undisturbed boundary-layer thickness δ_u. Therefore, the only possibility of altering $Re_{\delta u}$ is by means of δ_u variation. Several methods have been tested for this purpose. The one selected is drawn in Fig. 1; this is a step-slot arrangement, which allows a twofold action. One is a variable step height that influences the boundary-layer thickness substantially. The other is a flow injection along the wall, through the slot opened by the step. It is designed to provide a mass flow to the lower part of the boundary layer and thereby counteract the main-stream reattachment downstream of the step. This boundary-layer thickening arrangement has proved to be very effective in our experiments. It is important to mention that this arrangement does not introduce a spanwise nonuniformity into the boundary layer upstream of the interaction zone, and that flow injection is applied only at the highest Re case.

Pitot and static pressure surveys in the central plane are carried out by means of the vertical probe transport arrangement combined with a pressure data acquisition system. The static wall pressure is measured through taps of 0.5 mm diameter located along the centerline of the convex wall. Additional taps are located 10 mm off the centerline on both sides to check the symmetry of the flow. To provide a sufficient resolution of the pressure variation in the interaction area, the wall surface can be shifted in streamwise direction without wall shape variation. This allows pressure measurements in every desired location.

To determine shock topography and to control the flow repeatability by means of the shock location, a schlieren system is used. Photographs and a movie film are taken to analyze schlieren and oil-flow visualization.

Experimental Results of Shock-Induced Flow Separation

The following discussion focuses on the detection of flow separation. The measurements enable the determination of the boundary-layer velocity profiles and the subsequent calculation of the integral parameters and the determination of skin-friction values by means of a law-of-the-wall fit.[3,9] Let us at

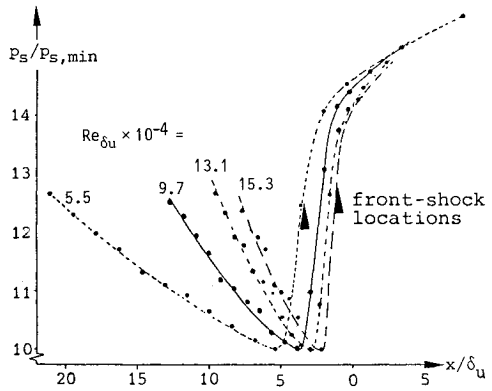

Fig. 3 Static-wall pressure distribution.

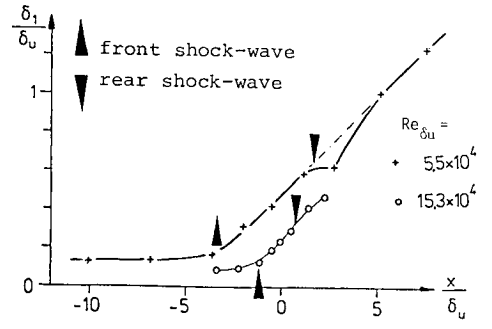

Fig. 4 Displacement thickness.

first relate the shock system to the measured static wall pressure distribution and the boundary-layer development up to flow separation.

Figure 2 shows the interaction zone by iso-Mach number lines for the case of $Re_{\delta u} = 5.5 \times 10^4$ and the shock system with the main normal shock and the front and rear branches of the λ-foot taken from a schlieren picture. A comparison of schlieren pictures taken with continuous and flash light has shown that shock unsteadiness is limited to very small amplitudes.

To investigate the Reynolds number effect on NSW/TBLI, the flowfield upstream of the interaction zone should not change. This is assured by keeping constant the wall Mach number M_w, calculated from the minimum static wall pressure and stagnation pressure upstream of the interaction. Due to the static pressure gradient normal to the wall, the flowfield maximum Mach number at the edge of the boundary layer changes a little with $Re_{\delta u}$ as δ_u is varied. The undisturbed boundary-layer thicknesses used in the present investigation are $\delta_u = 3.2$; 5.6; 7.6; 9.1 mm corresponding to $Re_{\delta u} \times 10^{-4} = 5.5$; 9.7; 13.1; 15.3, respectively. The wall Mach number chosen is $M_w = 1.47$.

The static wall pressure distributions for all investigated Reynolds numbers are presented in Fig. 3. These curves are arranged so that $x/\delta_u = 0$ refers to the normal projection of the main-shock position (taken from the schlieren picture) onto the wall. For the two extreme $Re_{\delta u}$ values the front-shock locations are indicated. These are obtained by extrapolation of the front branch onto the wall. Following arguments based on a two-dimensional interpretation of the static wall pressure distributions shown in Fig. 3, one is led to expect flow separation to occur where the pressure gradient starts to decrease after its first rapid increase.

Distributions of the displacement thickness δ_1 for the two extreme $Re_{\delta u}$ cases are presented in Fig. 4. The curves are again arranged so that the main-shock location corresponds to $x/\delta_u = 0$. The static-pressure jump at the wall causes the increase of δ_1 that reaches its maximum gradient just downstream of the front-shock location. This maximum gradient remains constant further downstream. This is another obser-

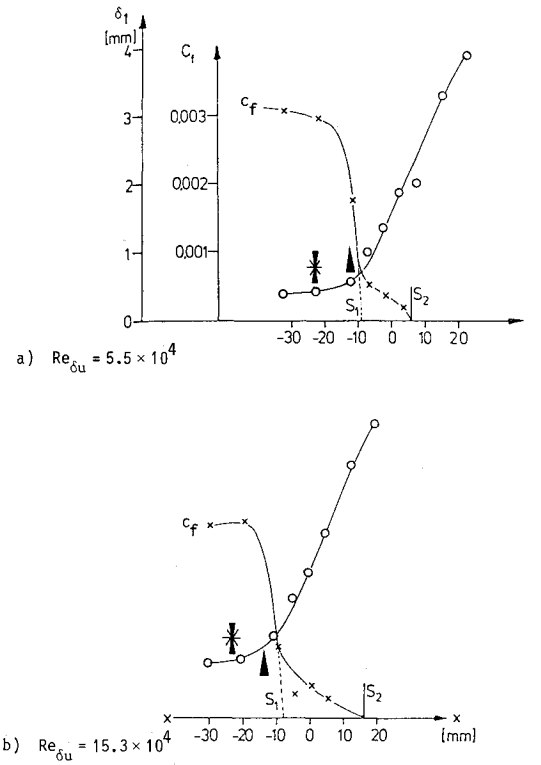

Figs. 5a and 5b Variation of boundary-layer displacement thickness δ_1 and skin-friction coefficient c_f along streamwise direction x (centerline) for the two extreme $Re_{\delta u}$ cases. Arrows indicate front-shock location, star indicates location of static wall pressure minimum.

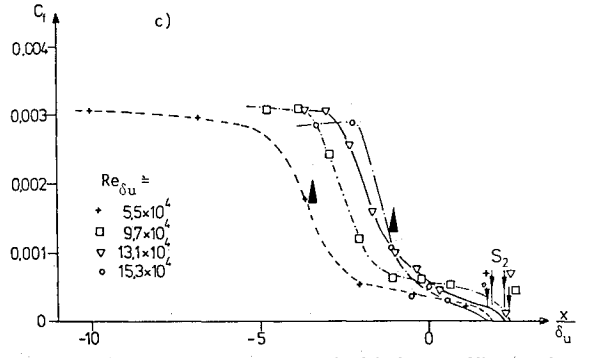

Fig. 5c Comparison of the varying skin-friction coefficients for the four investigated $Re_{\delta u}$ cases. Arrows indicate the front-shock locations only for the two extreme $Re_{\delta u}$ cases.

vation that is usually connected to boundary-layer separation in terms of a two-dimensional flow interpretation.

The other parameter that is important for separation detection is the skin-friction coefficient c_f. The c_f distribution is presented in Fig. 5 for all four $Re_{\delta u}$ cases. The curves are again arranged so that the main shock is placed at $x/\delta_u = 0$. The front-shock location is again indicated for the two extreme $Re_{\delta u}$ cases. The qualitative distribution behavior is the same for all cases. Upstream of the interaction, the c_f value curve is flat and is a little higher than $c_f = 0.003$; then, a sharp decrease takes place. In Figs. 5a and 5b it is indicated that this c_f drop and the simultaneous increase of δ_1 are connected to the locations of the static wall pressure minimum and the front shock. The most striking behavior (from a "two-dimensional point of view") is that the c_f drop is stopped before c_f reaches zero and the curves level out at very low values. This low c_f value decreases slowly further on to reach zero far downstream of the shock system. In a two-dimensional separated flow, the c_f drop should continue until negative values are reached within a separation bubble. After reaching a minimum, c_f should increase again to positive values through the reattachment point. It could be observed that, if the sharp c_f drop is extrapolated to $c_f = 0$, this location would coincide with a location where δ_1 reaches the maximum increase. This location is just downstream of the front shock and is indicated by S_1 in Fig. 5 (see also Fig. 2).

The obvious disagreement between the indication of flow separation by the skin friction ($c_f = 0$) and the displacement thickness and static wall pressure behavior, as well as the sharp c_f drop, followed by a c_f plateau, indicate that the separation structure is probably strongly influenced by three-dimensional flow effects.

Surface-Flow Visualization and Topology of the Three-Dimensional Flowfield

In order to clarify the problem, an oil-flow visualization has been applied at the convex wall. For this purpose a silicon oil has been seeded with TiO_2 white powder to obtain better contrast on the black mat surface of the convex wall. The mixture has been sprayed by means of an air brush producing only a thin layer on the convex wall surface. The obtained skin-friction line patterns for all $Re_{\delta u}$ cases are presented in Fig. 6a together with their topological interpretation sketched in Fig. 6b. It is clearly seen in Fig. 6a that oil is advected even onto the side walls, although no oil film was initially put there. Within the narrow corner region we recognize some oil-flow resolution difficulties.

In each presented picture, a view onto the convex wall through the side wall window is presented. The flow direction is from left to right and is indicated by large arrows. The double line is drawn on the convex wall surface, normal to the side wall windows, and it denotes the front-shock wall position taken from the schlieren picture.

In Fig. 6 there is one feature to be seen immediately in the structure of the observed skin-friction lines due to the changes of the Reynolds number: there is an asymmetry of the pattern, which increases substantially with a $Re_{\delta u}$ increase. Before we discuss this important feature, let us analyze the surface-flow patterns.

For a discussion of the wall pattern, it is convenient to use the visualization and the sketch given in Fig. 6 for $Re_\delta = 15.3 \times 10^4$. The beginning of the static wall pressure increase takes place between tap Nr. 10 and tap Nr. 11. At this location the first effect of the interaction is observed. It takes place in the convex-wall/side-wall corner, and causes a strong flow contraction. This contraction continues through the front-shock location. At about tap 13 the strong increase of the displacement thickness starts, and at about tap 14 the boundary layer should separate if the c_f drop were to be extrapolated to $c_f = 0$. However, the flow contraction is continued beyond this area. Further downstream, the skin-friction lines turn apart and are driven into two foci FS_1 and FS_2 before a separation saddle point S_2 is approached. This saddle has shifted off the centerline of the tunnel. The saddle S_2 is located far downstream of the shock system for all cases (see Fig. 2). This location is also marked on Fig. 5 and indicates that the c_f distribution obtained from velocity profiles is in agreement with the visualizations. Together with the degree of asymmetry, the location of S_2 is changed in reference to the front-shock location. For smaller $Re_{\delta u}$, i.e., for thinner boundary layers, the separation saddle S_2 is nearer to the front shock.

Based on two-dimensional considerations of NSW/TBLI, one is led to identify straight lines of separation and attachment, respectively. Their distance from each other, the so-called separation length, then provides a measure for the strength of NSW/TBLI. It is evident from Fig. 6 that one has to completely renounce such ideas of two-dimensional flow separation, at least in the case of NSW/TBLI investigated in such narrow wind tunnels.

One important feature of oil-flow visualization is that it provides (apart from technical problems) a complete time-averaged wall shear stress topology. However, for the defini-

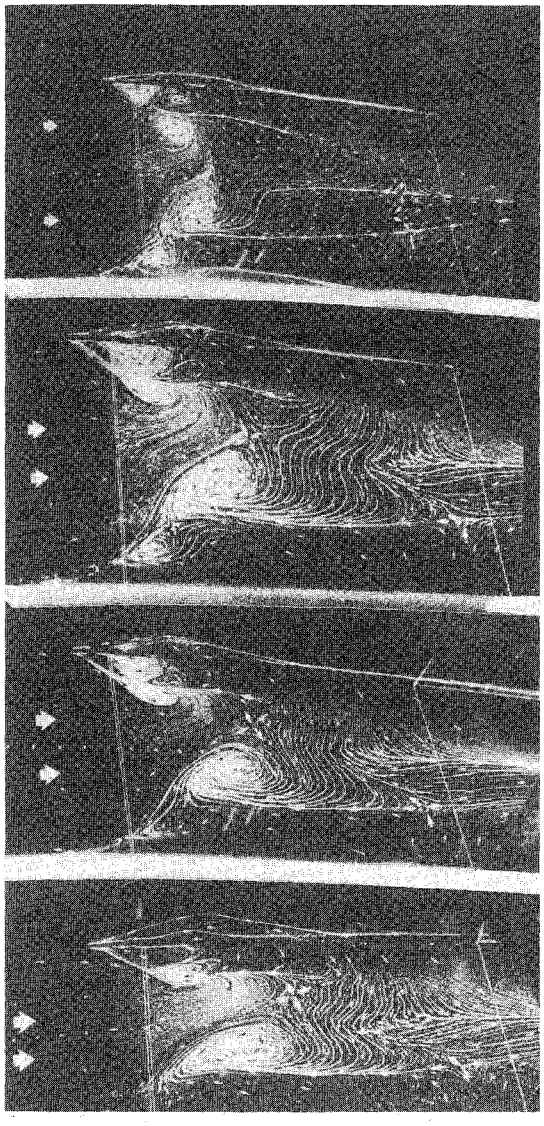

Fig. 6a Oil-flow visualizations (from top to bottom: $Re_{\delta u} \times 10^{-4} = 5.5, 9.7, 13.1$ and 15.3).

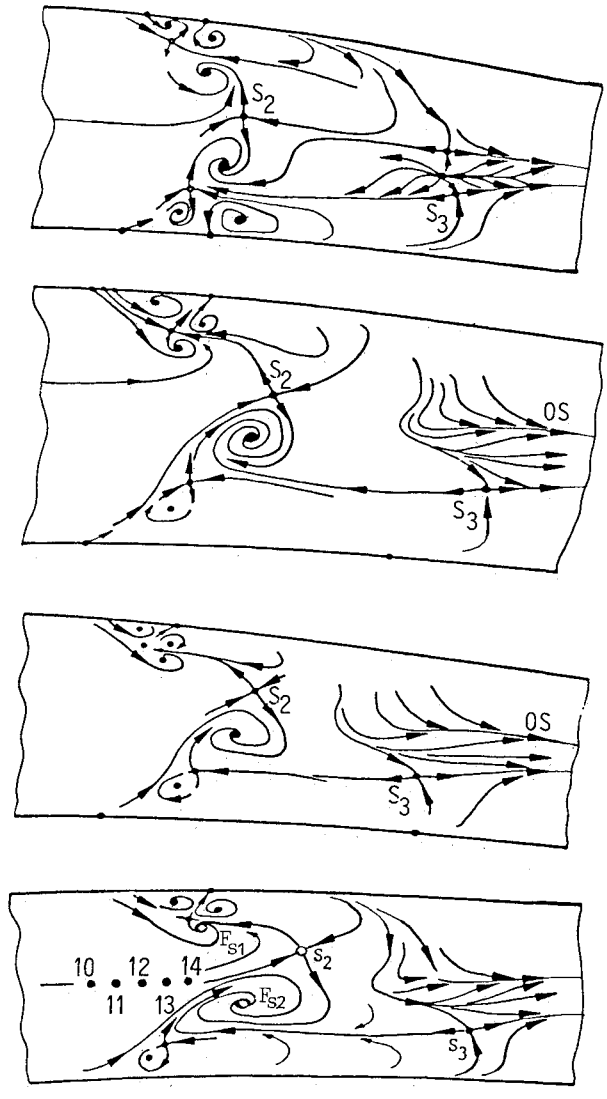

Fig. 6b Topological structures of surface flows shown in Fig. 6a.

tion of the topological flow structure of the time-averaged flowfield, we would have to identify all the so-called critical points within the whole three-dimensional flowfield. Oil-flow visualization only permits us to locate the critical points in the surface-flow pattern, i.e., all the points where the wall shear stress trajectories do not follow uniquely defined directions and where the wall shear stress magnitude is zero. At such points streamlines leave or reach the walls (see Legendre,[10] Lighthill,[11] Oswatitsch,[12] Peake and Tobak,[13] Perry and Fairlie,[14] Dallmann,[15-18] Chapman[19]). Hence, in the vicinity of each critical point a local flowfield topology can be deduced. Since a finite number of certain elementary topological structures (see Dallmann[20]) is formed by the flows between ensembles of critical points, a finite number of structurally stable flow configurations can also be conjectured. The topological description of the two-dimensional surface flow is a necessary but not a sufficient tool to conjecture a unique, three-dimensional flowfield topology. Hence, oil-flow visualizations are useful and important within these limits.

We follow the connections of critical points in Fig. 6. In the most symmetrical surface flow ($Re_{\delta u} = 5.5 \times 10^4$) we can identify a "separation line" that indicates strong convergence of wall shear stress trajectories and the location where the flow leaves the vicinity of the wall. In Fig. 7a it is sketched again as the thick line between $S-S$ that connects saddle points and foci.

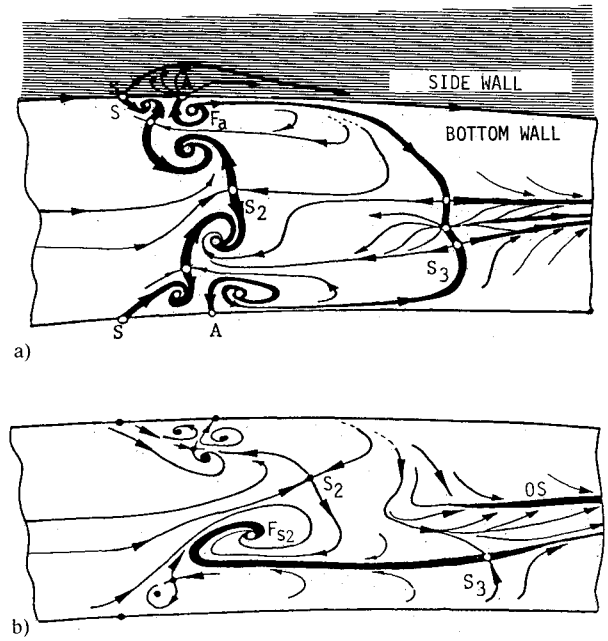

Fig. 7 "Separation lines" and "attachment line" (thick lines) identified in Fig. 6. a) $Re_{\delta u} = 5.5 \times 10^4$, b) $Re_{\delta u} = 15.3 \times 10^4$.

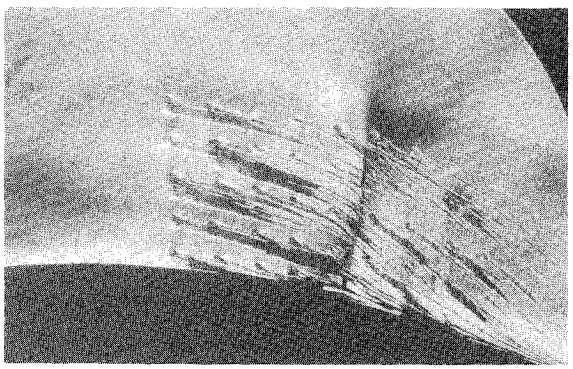

Fig. 8 Photograph of oil-dot visualization at a tunnel side wall (window) with schlieren system on to show the shock wave.

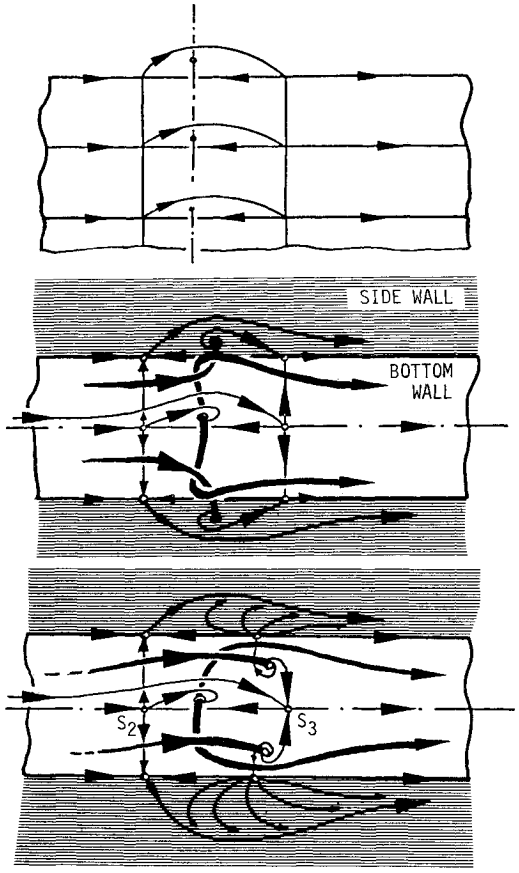

Fig. 9 Formation of a three-dimensional separated interaction zone bifurcating from a two-dimensional flow structure (separation bubble).

This "separation line" can be identified in all the other $Re_{\delta u}$ cases, although it becomes more and more deformed. An "attachment line" could be identified between $A-A$ where the flow appears to reach the wall. But for all the Reynolds numbers, especially for the highly asymmetric cases, another "separation line" appears along F_2-S_3 (Fig. 7b) and downstream of S_3. The time-averaged flow may either leave or reach the bottom wall at S_3. This indicates that there is no unique flow interpretation based only on surface flow patterns, i.e., there is no unique relationship between wall shear stress and three-dimensional flowfield topology (Dallmann[16,20]). We shall pay attention to this difficulty later in this paper. In Fig. 7a we also show that there is actually no flow reattachment at A since all the wall shear stress trajectories on the side wall leave the bottom wall at A, although they gradually approach the corner further downstream. There is local flow attachment at the focus F_a. In the downstream region of S_3 one also identifies for the higher $Re_{\delta u}$ cases a so-called "open separation" (OS), where only gradual convergence of wall shear stress trajectories indicates that the flow leaves the vicinity of the wall.[11]

There is evidence that a streamwise helical flow exists within the channel due to three-dimensional separation and, possibly, also due to the bottom wall curvature. Figure 8 presents an oil-dot visualization on a side wall with an instantaneous schlieren picture that shows the shock-wave location. It is evident that the flow direction at the side wall is inclined toward the convex wall. Downstream of the shock the inclination is much more pronounced. Since we recognize in Fig. 6 that the surface flow downstream of the interaction region converges toward the centerline while it approaches the curved wall along the sidewalls from above (according to Fig. 8), we conjecture streamwise oriented vortices to exist.

Reynolds Number Effect on Flowfield Structure and Symmetry

According to theoretical results on two-dimensional NSW/TBLI,[1,2] an increase of Reynolds number shortens the length of the shock-induced separation bubble. An interesting additional feature of the Reynolds number effect on our three-dimensional NSW/TBLI is the increasing asymmetry of the flow that is obvious in the surface-flow patterns of Fig. 6. This asymmetry could be caused by the asymmetry of the oncoming boundary layer. However, this idea is not supported by the static wall pressure measurements across the convex wall upstream of the interaction. A more convincing reason appears to lie in the tendency of the complex shear layer to roll up asymmetically around streamwise oriented vortices that form due to the three-dimensionality of the NSW/TBLI under consideration. This complex three-dimensionality of the separated flow region will be considered next.

We simplify the topological analysis and only discuss the time-averaged flow. We may stretch the surface-flow pattern to an arbitrary degree without changing the flow topology by not changing the critical point connections. Let us start with an idealized interaction that could cause a perfectly two-dimensional separation bubble (Fig. 9a). Of course no such possibility is provided in a wind tunnel experiment where side walls always cause three-dimensional perturbations in the flow. By arbitrarily small, three-dimensional perturbations, such a closed separation bubble can be broken up by a finite number of topologically different elementary flow changes.[20] The wall shear stress will not be zero along the whole separation and reattachment lines but it will vanish at isolated critical points. Local flow bifurcations create certain ensembles of critical points. Global bifurcations change the connections of critical points and herewith the global topology of the so-called singular stream surfaces[20] that define the three-dimensional flow structure. Two successive changes can be followed from Figs. 9a to 9b to 9c. All of these flows are still symmetrical with respect to the central plane. But one symmetrical pattern (Fig. 9c) exhibits a saddle-saddle connection S_2-S_3 along the centerline. Even arbitrarily small, localized disturbances can split this S_2-S_3 connection. This is a structural instability that can lead to a global topological change to asymmetric flow. The additional critical points seen in Fig. 6 (and those sketched in Fig. 7) along the "separation line" $S-S$ and near S_3 are formed by successive local bifurcations of the simple flow sketched in Fig. 9c. Hence, the structurally unstable configuration (Fig. 9c) can either bifurcate to the flow patterns seen in Fig. 6 (and Fig. 7) or to a different but also stable symmetrical pattern (that does not appear in our experiment). This indicates that the structurally stable asymmetric surface flow (where S_2 is not connected to S_3) is a consequence of a hydrodynamic instability of the three-dimensional NSW/TBLI. It is possible that there is another range of Reynolds numbers where structurally and hydrodynamically stable, symmetric flow configurations exist. We again emphasize that the asymmetry is not forced by asymmetric boundary-layer thickening upstream of the interaction re-

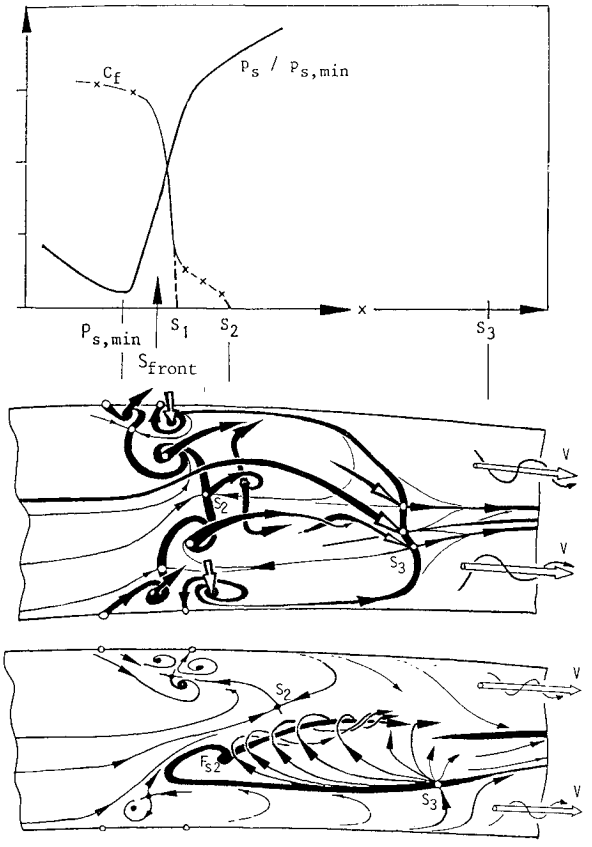

Fig. 10 Conjectured three-dimensional flowfield structures based on Fig. 7 with a) flow reattachment at S_3 and b) flow separation at S_3. The streamwise oriented vortical flow V downstream of the interaction region is conjectured from Figs. 6 and 8.

gion. The first disturbances to enter the separated flow region at the side-wall/bottom-wall corners appear perfectly symmetrical. We want to mention that high Reynolds number flows with separated, three-dimensional, streamwise vortices often show a staggered, asymmetric flow structure.

Various kinematically possible flowfield structures can be conjectured from each of the surface flows given in Fig. 6. We sketch only two of them in Figs. 10a and 10b following the above given discussion of Fig. 7 for the two extreme $Re_{\delta u}$ cases. At the downstream saddle S_3 the time-averaged flow may attach but also leave the wall. The complex swirling motions that arise in the interaction region carry vorticity and interact by Biot-Savart's law to result in the streamwise oriented vortices V sketched in Fig. 10 in the downstream region.

In Fig. 10 (top) we also show how the static wall pressure rises, the skin-friction drops, and the skin-friction plateau is related to the complex flow structure. This points out the difficulty of defining a single "separation length" that could characterize the Reynolds number effect on the interaction.

On the Definition of Interaction Length Scales

The strength of two-dimensional NSW/TBLI is usually characterized by the length of the associated separation bubble. In wind tunnels much wider than ours, separation may be indicated by almost straight lines that form normally to the oncoming stream in the central part of those tunnels. Nevertheless, the separated flow region itself is always three-dimensional, including a highly curved reattachment line.

In two-dimensional as well as in our three-dimensional cases, the beginning of NSW/TBLI has to be considered where the static wall pressure attains a minimum (indicated in Fig. 10 as $P_{s,min}$). From $P_{s,min}$ on we also observe a gradual increase of δ_1 (Fig. 4) and a sharp decrease of c_f (Fig. 5c) without c_f going to zero necessarily. The relative location of characteristic points of the flowfield is sketched in Fig. 10

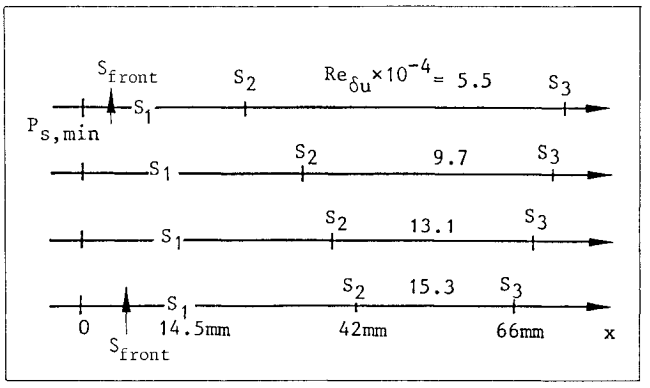

Fig. 11 Interaction length scales

(top). It is to be mentioned that some other experimenters report "separation" to have taken place where a sudden c_f drop is observed and $c_f = 0$ is reached immediately. They find that separation takes place within the visualized foot of the shock. This is not the case here. The location of the separation saddle point S_2 is highly influenced by the strength of the neighboring vortex system that forms near the side walls, and which depends on the Reynolds number.

Thus, it appears to the authors that one could characterize the Reynolds number effect on the strength of such three-dimensional NSW/TBLI only by relating the locations of

1) minimum static wall pressure ($P_{s,min}$),
2) front shock (S_{front}),
3) (sudden) drop of wall shear stress (S_1),
4) upstream separation saddle point (S_2), and
5) downstream saddle point (S_3) or another downstream limit of the interaction zone.

In addition the asymmetry of the interaction has to be characterized.

Figure 10 (top) provides the definition of NSW/TBLI-length scales, which we then measure from Figs. 3, 5, and 6 and display them in Fig. 11. Because of the apparent three-dimensionality of the NSW/TBLI, it is meaningless to compare Fig. 11 with the "separation (bubble) lengths" published by other authors. Nevertheless, we recognize that the distance $S_2 - S_3$ decreases as one increases the Reynolds number. This is in formal agreement with two-dimensional results[1,2] (where the distance $S_2 - S_3$ would define the separation bubble length). The separated flow region within the central part of the channel is considerably shifted downstream as one increases $Re_{\delta u}$, away from the minimum static wall pressure and away from the skin-friction drop.

Conclusions

An experimental and topological investigation of NSW/TBLI on a convex plate in a narrow wind tunnel performed at $M_w = 1.47$ and in a range $5.5 \times 10^4 \leq Re_{\delta u} \leq 15.3 \times 10^4$ has revealed the following:

1) The flowfield within the separated zone caused by the interaction is highly three-dimensional.

2) Due to this three-dimensionality, there is a peculiar behavior observed in the skin-friction distribution c_f along the channel center plane. A sharp c_f drop is observed where a sharp static-pressure rise is measured. However, the actual separation where the boundary-layer flow leaves the vicinity of the wall is found much further downstream.

3) An investigation of flow topology based on the visualizations together with the measurements of static wall pressure, pitot and static pressure surveys above the wall, and schlieren pictures provides an explanation of the observed interaction phenomena.

4) There is a preference to asymmetry that is considerably enhanced as the Reynolds number is increased. This asymmetry is not present in the oncoming boundary layer, but seems to result from global flow instability when streamwise

oriented, separated shear layers and vortices are formed by NSW/TBLI in the wind tunnel.

5) No single separation length scale could be defined to characterize NSW/TBLI in a narrow wind tunnel.

Acknowledgments

The authors are indebted to Professor J. Zierep, who made possible the experiments and the stay of one of the authors at his institute. Also, the experimental supports provided by Dr. H. Jungbluth and Dr. Habil R. Bohning are greatly appreciated.

References

[1]Bohning, R. and Zierep, J., "Normal Shock Turbulent Boundary-Layer Interaction at a Curved Wall," *Computation of Viscous-Inviscid Interactions,* AGARD CP-291, 1980, pp. 17-1—17-8.

[2]Bohning, R., "Die Wechselwirkung eines senkrechten Verdichtungsstosses mit einer turbulenten Grenzschicht an einer gekrümmten Wand," Inaugural dissertation, Karlsruhe, Universität (TH), Habilitationsschrift, 1982.

[3]Doerffer, P. and Zierep, J., "An Experimental Investigation of the Reynolds Number Effect on a Normal Shock Wave-Turbulent Boundary Layer Interaction on a Curved Wall," *Acta Mechanica,* Vol. 73 pp. 77-93.

[4]Nebbeling, C., "An Experimental Investigation of the Interaction Between a Shock Wave and a Turbulent Boundary Layer on a Convex Wall," Delft Univ. of Technology, Dept. of Aerospace Engineering, Rept. LR-428, 1984.

[5]Benay, R., Pot, R., and Délery, J., "Experimental Analysis of the Flow Through a Three Dimensional Transonic Channel," *Rech. Aérospace*, No. 1986-6, 1986, pp. 11-26.

[6]Doerffer, P., "An Experimental Stand and Measurement Methods to be Used in Turbulent Boundary Layer-Normal Shock Wave Interaction on a Curved Wall," Strömungsmechanik und Strömungsmaschinen 35/85, Universität Karlsruhe, 1985.

[7]Doerffer, P., "The Compression Zone Topography in the Normal Shock Wave-Turbulent Boundary Layer Interaction," Strömungsmechanik und Strömungsmaschinen 38/86, Universität Karlsruhe, 1986.

[8]Doerffer, P., "Boundary Layer Pressure Distribution Measurements in a Transonic Wind Tunnel," Strömungsmechanik und Strömungsmaschinen 35/85, Universität Karlsruhe, 1985.

[9]Doerffer, P., "An Experimental Investigation of a Normal Shock Wave and a Turbulent Boundary Layer Interaction at a Curved Wall for: $M_w = 1.47$; $Re_{\delta u} = 1.53 \times 10^5$," Strömungsmechanik und Strömungsmaschinen 38/86, Universität Karlsruhe, 1986.

[10]Legendre, R., "Séparation De L'Ecoulement Laminaire Tridimensionnel," *La Recherche Aéronautique*, No. 54, Nov.-Dec. 1956.

[11]Lighthill, M. J., "Attachment and Separation in Three-Dimensional Flow," *Laminar Boundary Layers,* edited by L. Rosenhead, II, 2.6, Oxford Univ. Press, 1963, pp. 72-82.

[12]Oswatitsch, K., "Die Ablösungsbedingung von Grenzschichten," *IUTAM Symposium on Boundary Layer Research,* edited by H. Goertler, Springer-Verlag, Freiburg, FRG, Aug. 1958.

[13]Peake, D. J. and Tobak, M., "Three-Dimensional Interactions and Vortical Flows with Emphasis on High Speeds," AGARD AG-252, July 1980.

[14]Perry, A. E. and Fairlie, B. D., "Critical Points in Flow Patterns," *Advances in Geophysics,* Vol. 18B, Academic, New York, San Francisco, London, 1974, p. 299-315.

[15]Dallmann, U., "Topological Structures of Three-Dimensional Flow Separations," DFVLR-IB 221-82 A 07, 1983.

[16]Dallmann, U., "Topological Structures of Three-Dimensional Flow Separations," AIAA Paper 83-1735, July 1983.

[17]Dallmann, U., "On the Formation of Three-Dimensional Vortex Flow Structures," DFVLR-IB 221-85 A 13, 1985.

[18]Dallmann, U., "Structural Stability of Three-Dimensional Vortex Flows," *Nonlinear Dynamics in Transcritical Flows,* edited by H. L. Jordan, H. Oertel, and K. Robert, Springer Lecture Notes in Engineering, Bonn, 1985.

[19]Chapman, G. T., "Topological Classification of Flow Separation on Three-Dimensional Bodies," AIAA Paper 86-0485, Jan. 1986.

[20]Dallmann, U., "Three-Dimensional Vortex Structures and Vorticity Topology," *IUTAM Symposium on Fundamental Aspects of Vortex Motion,* Tokyo, 1987, Fluid Dynamics Research 3, The Japan Society of Fluid Mechanics, North-Holland Physics Publ., edited by H. Hasimoto and T. Kambe, 1988, pp. 183-189.